Generalized arcsine laws for fractional Brownian motion

Tridib Sadhu, Mathieu Delorme, Kay Jörg Wiese

Generalized arcsine laws for fractional Brownian motion

Tridib Sadhu,[1] Mathieu Delorme,[2] and Kay Jörg Wiese[2]

[1] *Tata Institute of Fundamental Research, Mumbai 400005, India.*
[2] *Laboratoire de Physique Théorique, Département de Physique de l'ENS, Ecole Normale Supérieure, 24 rue Lhomond, 75005 Paris, France. CNRS; PSL Research University; UPMC Univ. Paris 6, Sorbonne Universités.*

The *three arcsine laws* for Brownian motion are a cornerstone of extreme-value statistics. For a Brownian B_t starting from the origin, and evolving during time T, one considers the following three observables: (i) the duration t_+ the process is positive, (ii) the time $t_{\rm last}$ the process last visits the origin, and (iii) the time $t_{\rm max}$ when it achieves its maximum (or minimum). All three observables have the same cumulative probability distribution expressed as an arcsine function, thus the name of *arcsine laws*. We show how these laws change for fractional Brownian motion X_t, a non-Markovian Gaussian process indexed by the Hurst exponent H. It generalizes standard Brownian motion (*i.e.* $H = \frac{1}{2}$). We obtain the three probabilities using a perturbative expansion in $\varepsilon = H - \frac{1}{2}$. While all three probabilities are different, this distinction can only be made at second order in ε. Our results are confirmed to high precision by extensive numerical simulations.

PACS numbers: 05.40.Jc, 02.50.Cw, 87.10.Mn

The three arcsine laws for Brownian motion or more generally for discrete random processes [1–4] are celebrated properties of stochastic processes. For a Brownian B_t starting from the origin, and evolving during time T, one considers the following three observables (see Fig. 1): (i) the total duration t_+ when the process is positive, (ii) the last time $t_{\rm last}$ the process visits the origin, and (iii) the time $t_{\rm max}$ it achieves its maximum (or minimum). Remarkably, all three observables have the same probability distribution as a function of $\vartheta := t/T$,

$$p(\vartheta) = \frac{1}{\pi\sqrt{\vartheta(1-\vartheta)}} \ . \tag{1}$$

As the cumulative distribution contains an arcsine function, these laws are commonly referred to as the *first, second* and *third* arcsine law. These laws apply quite generally to Markov processes, *i.e.* processes where the increments are uncorrelated [2]. Their counter-intuitive form with a divergence at $\vartheta = 0$ and $\vartheta = 1$ has sparked a lot of interest, and they are considered among the most important properties of stochastic processes. Recent studies led to many extensions, in constrained Brownian motion [5–7], for general stochastic processes [8–13], even in higher dimensions [14–16]. The laws are realized in a plethora of real-world examples, from finance [17, 18] to competitive team sports [19].

In this *letter*, we ask how these laws change for fractional Brownian motion (fBm) which is a generalization of standard Brownian motion preserving scale invariance as well as translation invariance, both in time and space. FBm was introduced in its final form by Mandelbrot and Van Ness [20] to describe time-series data in natural processes. It is defined as a Gaussian process X_t, starting at zero, $X_0 = 0$, with mean $\langle X_t \rangle = 0$ and covariance

$$\langle X_t X_s \rangle = t^{2H} + s^{2H} - |t-s|^{2H} \ . \tag{2}$$

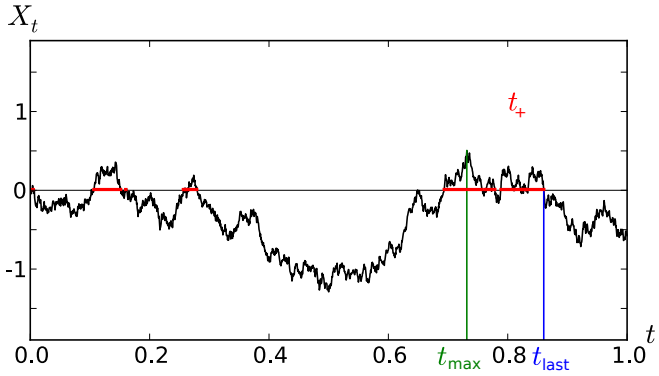

FIG. 1. The three observables t_+, $t_{\rm last}$, and $t_{\rm max}$ considered in this letter.

The parameter $H \in (0, 1)$ is the Hurst exponent. Standard Brownian motion corresponds to $H = \frac{1}{2}$ where the covariance reduces to $\langle X_t X_s \rangle = 2\min(s, t)$. Unless $H = \frac{1}{2}$, the process is non-Markovian, *i.e.* its increments are not independent. For $H > \frac{1}{2}$ they are positively correlated, while for $H < \frac{1}{2}$ they are anti-correlated. This non-Markovian nature makes a theoretical analysis of fBm difficult, and only few exact results are available in the literature [21–23].

FBm is important as it successfully models a variety of natural processes [24]: a tagged particle in the single-file ($H = 0.25$) [25, 26], the integrated current in diffusive transport ($H = 0.25$) [27], polymer translocation through a narrow pore ($H \simeq 0.4$) [28–30], anomalous diffusion [31], values of the log return of a stock ($H \simeq 0.6$ to 0.8) [32–35], hydrology ($H \simeq 0.72$ to 0.87) [36], a tagged monomer in a polymer ($H = 0.25$) [37], solar flare activity ($H \simeq 0.57$ to 0.86) [38], the price of electricity in a liberated market ($H \simeq 0.41$) [39], telecommunication networks ($H \simeq 0.78$ to 0.86) [40], telomeres

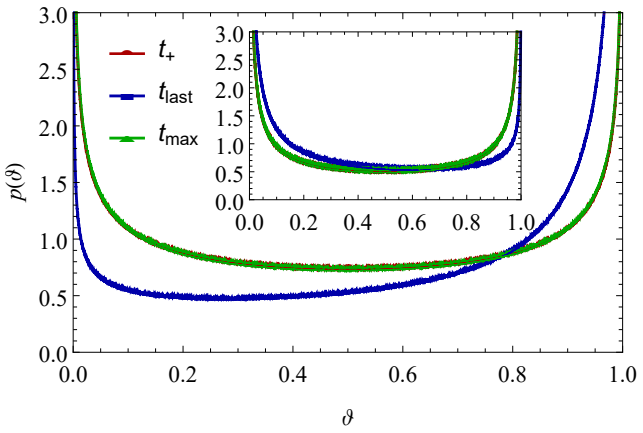

FIG. 2. Numerical simulation results for the probability of the three observables $t_{\rm last}$, t_+, and $t_{\rm max}$ for a fBm with $H = 0.33$. The inset shows the probabilities for $H = 0.66$. Note that the distributions of t_+ and $t_{\rm max}$ are almost indistinguishable.

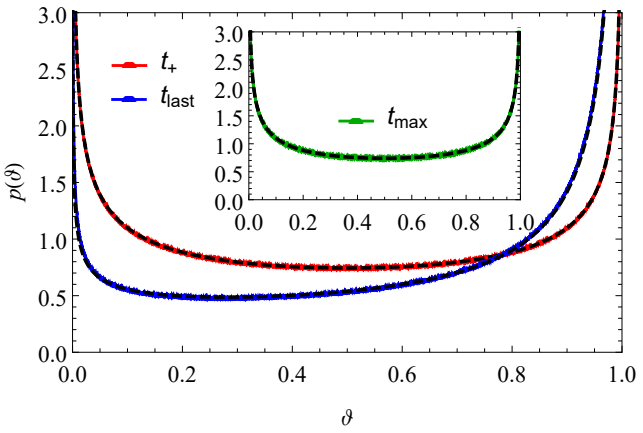

FIG. 3. Comparison of the formulas (3)-(5) with their corresponding numerical simulation result of a fBm with $H = 0.33$. The dashed lines are the theoretical result. $p_{\rm max}(\vartheta)$ is shown in the inset as it is almost indistinguishable from $p_+(\vartheta)$.

inside the nucleus of human cells ($H \simeq 0.18$ to 0.35) [41], or diffusion inside crowded fluids ($H \simeq 0.4$) [42]. Generalizing the three arcsine laws (1) to fBm thus has fundamental importance, as well as a multitude of potential applications.

Unlike for Brownian motion, the probabilities of the three observables t_+, $t_{\rm last}$ and $t_{\rm max}$ are different. Using an expansion in $\varepsilon = H - \frac{1}{2}$, we derive them in the form:

$$p_+(\vartheta) = \frac{\mathcal{N}_+}{[\vartheta(1-\vartheta)]^H}\, \mathrm{e}^{\varepsilon \mathcal{F}_1^+(\vartheta) + \varepsilon^2 \mathcal{F}_2^+(\vartheta) + \mathcal{O}(\varepsilon^3)} \tag{3}$$

$$p_{\rm last}(\vartheta) = \frac{\mathcal{N}_{\rm last}}{\vartheta^H (1-\vartheta)^{1-H}}\, \mathrm{e}^{\varepsilon \mathcal{F}_1^{\rm last}(\vartheta) + \varepsilon^2 \mathcal{F}_2^{\rm last}(\vartheta) + \mathcal{O}(\varepsilon^3)} \tag{4}$$

$$p_{\rm max}(\vartheta) = \frac{\mathcal{N}_{\rm max}}{[\vartheta(1-\vartheta)]^H}\, \mathrm{e}^{\varepsilon \mathcal{F}_1^{\rm max}(\vartheta) + \varepsilon^2 \mathcal{F}_2^{\rm max}(\vartheta) + \mathcal{O}(\varepsilon^3)} \tag{5}$$

The pre-factors of the exponential are predicted using scaling arguments for $\vartheta \to 0$ and $\vartheta \to 1$. The terms in the exponential are non-trivial, and finite over the full range of ϑ. We use the convention that the integral over each $\mathcal{F}$-function vanishes, which adjusts the normalization constants $\mathcal{N}$. To leading order we find

$$\begin{aligned} \mathcal{F}_1^+(\vartheta) &= \mathcal{F}_1^{\rm max}(\vartheta) \\ &= \pi \sqrt{\frac{1-\vartheta}{\vartheta}} + \frac{2(2\vartheta - 1)\,\mathrm{acos}(\sqrt{\vartheta})}{\sqrt{(1-\vartheta)\vartheta}} - \frac{\pi^2}{2} + 2\ , \end{aligned} \tag{6}$$

$$\mathcal{F}_1^{\rm last}(\vartheta) = 0\ . \tag{7}$$

The expression of $\mathcal{F}_1^{\rm max}(\vartheta)$ was reported earlier [43–46]. The equality of $\mathcal{F}_1^+$ and $\mathcal{F}_1^{\rm max}$, and their difference from the vanishing $\mathcal{F}_1^{\rm last}$ is qualitatively seen in Fig. 2. We have no intuitive understanding of this coincidence.

A numerical estimation of the three probabilities is obtained using a discrete-time algorithm [47] for fBm of a given H, which generates sample trajectories drawn from a Gaussian probability with covariance (2). The probabilities in figures 2 and 3 are obtained by averaging over 5×10^9 sample trajectories, each with 2^{13} time steps.

Figure 2 shows that $p_{\rm last}(\vartheta)$ behaves markedly differently from the other two distributions; especially, it is asymmetric under the exchange $\vartheta \to 1-\vartheta$. This can be seen in the scaling part of Eq. (4), where the exponent H comes from the return probability to the starting point, while the survival exponent $\theta = 1 - H$ governs the divergence for $\vartheta \to 1$. This asymmetry in exponents is reversed around $H = \frac{1}{2}$, as seen in the inset of figure 2.

The analytical expressions for $\mathcal{F}_2$ in Eqs. (3)–(5) are cumbersome; we will sketch the derivation for the simplest one, $\mathcal{F}_2^{\rm last}(\vartheta)$, below, while the remaining ones will be reported elsewhere [48].

Confirmation of our theoretical results comes from comparison with numerical simulations of the probabilities presented in Fig. 3. For a finer comparison we plot our theoretical results of $\mathcal{F}_2(\vartheta)$ in Fig. 4 alongside their extraction from numerical simulations. To illustrate our procedure, we use Eq. (3) to define

$$\mathcal{F}_{2,\varepsilon}^+(\vartheta) := \frac{1}{\varepsilon}\left[\frac{1}{\varepsilon}\ln\left(p_+(\vartheta)\frac{[\vartheta(1-\vartheta)]^H}{\mathcal{N}^+}\right) - \mathcal{F}_1^+(\vartheta)\right]\ . \tag{8}$$

Then, $\mathcal{F}_{2,\varepsilon}^+(\vartheta) = \mathcal{F}_2^+(\vartheta) + \mathcal{O}(\varepsilon)$ which contains all terms in the exponential in Eq. (3) except $\mathcal{F}_1^+(\vartheta)$. One can improve this estimation by using that the sub-leading term in $\mathcal{F}_{2,\varepsilon}^+(\vartheta)$ is odd in ε, to define

$$\overline{\mathcal{F}}_{2,\varepsilon}^+(\vartheta) := \frac{1}{2}\Big[\mathcal{F}_{2,\varepsilon}^+(\vartheta) + \mathcal{F}_{2,-\varepsilon}^+(\vartheta)\Big] = \mathcal{F}_2^+(\vartheta) + \mathcal{O}(\varepsilon^2)\ . \tag{9}$$

A comparison of $\overline{\mathcal{F}}_{2,\varepsilon}^+(\vartheta)$ extracted from numerical simulations of $p_+(\vartheta)$ with the theoretical result of $\mathcal{F}_2^+(\vartheta)$ is plotted in Fig. 4 for $\varepsilon = \pm\frac{1}{6}$. The figure also contains the comparison for $\mathcal{F}_2^{\rm last}(\vartheta)$ and $\mathcal{F}_2^{\rm max}(\vartheta)$. As one

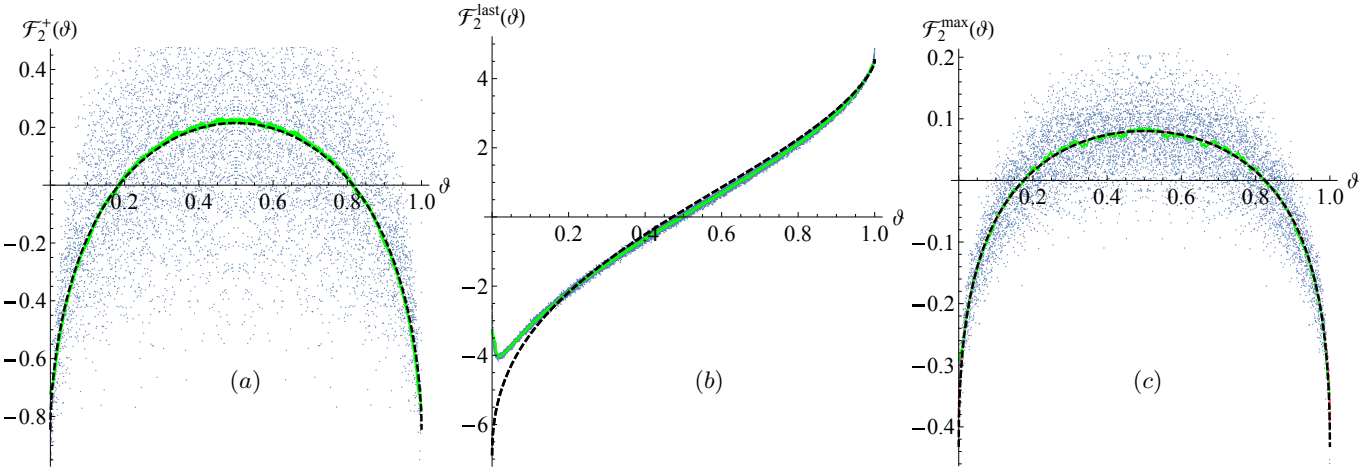

FIG. 4. A comparison for the three $\mathcal{F}_2(\vartheta)$ obtained analytically (black dashed lines) and their measurement using formula (9) with $\varepsilon = \pm\frac{1}{6}$. From left to right: (a) positive time, (b) time of the last visit to the origin, and (c) time for the maximum. The scattered dots are the raw data from trajectories of $N = 2^{13}$ time steps, averaged over 5×10^9 samples, which are coarse grained by a factor of 100 to give the green curve. Approximations of our analytical results are given in the supplementary material.

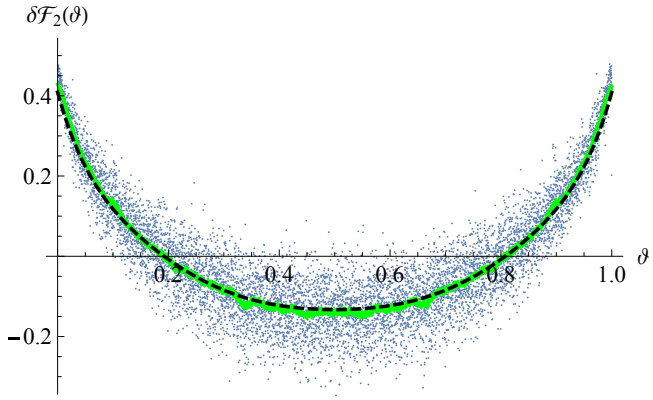

FIG. 5. The difference $\delta\mathcal{F}_2(\vartheta) = \mathcal{F}_2^{\rm max}(\vartheta) - \mathcal{F}_2^+(\vartheta)$, using the same conventions as in Fig. 4. This plot quantifies the difference between the first and third arcsine law.

sees, the agreement between theory and numerical simulations is quite striking: remind that these are sub-sub leading corrections, almost indiscernable in Fig. 3. We note the much larger amplitude of $\mathcal{F}_2^{\rm last}(\vartheta)$. The latter also has the largest deviations from the theory, especially for $\theta \to 0$. These deviations indicate the presence of subleading terms of order ε^4, or higher.

In Fig. 2 the probabilities $p_+(\vartheta)$ and $p_{\rm max}(\vartheta)$ are hard to distinguish from each other. Their difference can analytically be seen only at second order in ε. To underline that these are distinct distributions, we show the difference $\delta\mathcal{F}_2(\vartheta) = \mathcal{F}_2^{\rm max}(\vartheta) - \mathcal{F}_2^+(\vartheta)$ in Fig. 5.

In the rest of this letter we sketch the derivation of formulas (3)–(5). We begin with the action which characterizes the probability of a fBm trajectory,

$$\mathcal{S}[X] = \int_0^T {\rm d}t_1 \int_{t_1}^T {\rm d}t_2 \; \dot{X}_{t_1} \mathcal{C}^{-1}(t_1,t_2) \dot{X}_{t_2} \; . \qquad (10)$$

Here $\mathcal{C}(t_1,t_2)$ is the co-variance given in Eq. (2). We use an expansion [44, 49] of the action around $H = \frac{1}{2}$ to take advantage of the Markov property of Brownian motion. One writes

$$\mathcal{C}(t_1,t_2) = 2D_\varepsilon \left[\delta(t_1-t_2) + \frac{\varepsilon}{|t_1-t_2|} + \frac{2\varepsilon^2 \ln\left|\frac{t_1-t_2}{\tau}\right|}{|t_1-t_2|} + \mathcal{O}(\varepsilon^3) \right] \qquad (11)$$

which leads to an expansion of the action [50]

$$S[X] = \frac{1}{2D_\varepsilon} \int_0^T {\rm d}t_1 \int_{t_1}^T {\rm d}t_2 \; \dot{X}_{t_1} \dot{X}_{t_2} \Big[\delta(t_1-t_2) + \frac{\varepsilon}{|t_1-t_2|} + \int_{t_1}^{t_2} {\rm d}s \, \frac{\varepsilon^2}{|t_1-s|\,|t_2-s|} + \mathcal{O}(\varepsilon^3) \Big] \qquad (12)$$

where $D_\varepsilon \simeq (1+2\varepsilon)\tau^{2\varepsilon}$ and all expressions are regularized by an ultraviolet cutoff τ in time.

Our calculation for the probabilities is done in Laplace variables. One reason for this choice is that the space integrals appearing in perturbation theory are easier. A further advantage is that temporal convolutions become mere products in the conjugate Laplace-variables. The action (12) is written in Laplace variables [44] using

$$\frac{\Theta(|t_1-t_2|>\tau)}{|t_1-t_2|} \simeq \int_0^\Lambda {\rm d}y \, {\rm e}^{-y|t_1-t_2|} \; , \qquad (13)$$

where $\Theta(x)$ is the Heaviside function, and the UV cutoff Λ is related to τ by $\ln(\tau) = -\ln(\Lambda) - \gamma_{\rm E}$ with $\gamma_{\rm E}$ the Euler constant. As an explicit example, let us consider the calculation of $P_{\rm last}(t,T)$ and its Laplace transform

$$\widetilde{P}_{\rm last}(\lambda,s) = \int_0^\infty {\rm d}T \int_0^T {\rm d}t \, {\rm e}^{-\lambda t - sT} P_{\rm last}(t,T) \; . \qquad (14)$$

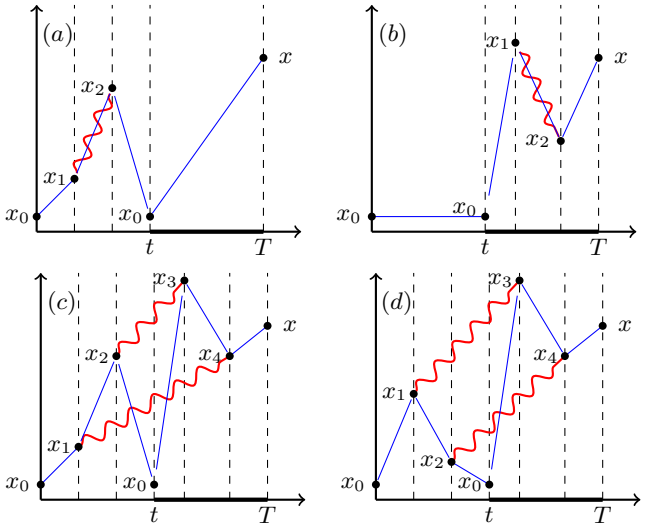

FIG. 6. The diagrams (a) and (b) contributing to the order-ε term in $p_{\rm last}(\vartheta)$, as well as (c) and (d) contributing to the order-ε^2 term $\mathcal{F}_2^{\rm last}(\vartheta)$ in (4). Solid lines denote the Brownian propagators, with absorbing boundary conditions indicated by a bold line after time t. The curly lines represent the order-ε interaction in Eq. (12).

The quantity of interest is $p_{\rm last}(\frac{t}{T}) = \frac{1}{T}P_{\rm last}(t,T)$ which yields

$$\widetilde{P}_{\rm last}(\lambda,s) = \frac{1}{s}\int_0^1 {\rm d}\vartheta\, \frac{p_{\rm last}(\vartheta)}{1+\kappa\vartheta}\ ; \quad \kappa = \frac{\lambda}{s}\ . \tag{15}$$

Defining $\widetilde{p}_{\rm last}(\kappa) := s\widetilde{P}_{\rm last}(\lambda,s)$, one obtains the probability $p_{\rm last}(\vartheta)$ by taking the inverse transformation

$$p_{\rm last}(\vartheta) = \lim_{\phi\to\pi}\frac{-1}{\pi\vartheta}\Im\,\widetilde{p}_{\rm last}(\kappa = {\rm e}^{i\phi}/\vartheta)\ , \tag{16}$$

where $\Im$ denotes the imaginary part. This is proven from Eq. (15) via analytical continuation.

The calculation is simplest at order zero in ε, *i.e*, for a Brownian. Using Eqs. (12) and (14) one writes

$$\widetilde{P}^{H=\frac12}_{\rm last}(\lambda,s) = \lim_{x_0\to 0}\frac{2}{x_0}\int_0^\infty {\rm d}x\,\widetilde{Z}(x_0,x_0,s+\lambda)\widetilde{Z}^+(x_0,x,s)\ . \tag{17}$$

Here $\widetilde{Z}(x,y,s) = (2\sqrt{s})^{-1}\exp(-\sqrt{s}|x-y|)$ is the Laplace transform of the Brownian propagator, while $\widetilde{Z}^+(x,y,s) = Z(x,y,s) - Z(x,-y,s)$ is the propagator in presence of an absorbing wall at the origin. This yields

$$\widetilde{p}^{H=\frac12}_{\rm last}(\kappa) = s\ \widetilde{P}^{H=\frac12}_{\rm last}(s\kappa,s) = \frac{1}{\sqrt{1+\kappa}}\ . \tag{18}$$

Using the transform (16) one obtains the arcsine law (1).

Perturbative corrections to the probability are evaluated by following a similar procedure [44]. Contributions at different orders in ε are represented by the diagrams in Fig. 6. The non-vanishing contributions at order ε come from the two diagrams (a) and (b) which like (17) are expressed in terms of the Brownian propagator. For example, the amplitude corresponding to diagram (a) is

$$\frac{4\varepsilon}{x_0}\int_0^\Lambda {\rm d}y\int_{-\infty}^\infty {\rm d}x_1\int_{-\infty}^\infty {\rm d}x_2\int_0^\infty {\rm d}x\,\widetilde{Z}(x_0,x_1,s_1) \tag{19}$$
$$\times\,\partial_{x_1}\widetilde{Z}(x_1,x_2,s_1{+}y)\partial_{x_2}\widetilde{Z}(x_2,x_0,s_1)\widetilde{Z}^+(x_0,x,s)$$

where $s_1 = s(1+\kappa)$. This leads to the non-trivial power-law in Eq. (4) and a vanishing $\mathcal{F}_1^{\rm last}$ in Eq. (7).

At order ε^2, there are multiple diagrams which contribute to the probability $\widetilde{p}_{\rm last}(\vartheta)$. However, the only contributions to $\mathcal{F}_2^{\rm last}$ come from the two diagrams (c) and (d) in Fig. 6. After some tedious algebra, the net amplitude of the two diagrams reads

$$\widetilde{\mathcal{F}}_2^{\rm last}(\kappa) = -\int_0^\Lambda {\rm d}y_1\,{\rm d}y_2\Big[\sqrt{\kappa{+}y_1{+}y_2{+}1} - \sqrt{\kappa{+}y_1{+}1}$$
$$-\sqrt{\kappa{+}y_2{+}1} + \sqrt{\kappa{+}1}\Big]\times\frac{2\sqrt{1{+}\kappa}\sqrt{y_1{+}y_2{+}1}}{y_1^2y_2^2}$$
$$\times\left(1-\sqrt{y_1{+}1}-\sqrt{y_2{+}1}+\sqrt{y_1{+}y_2{+}1}\right). \tag{20}$$

Finally, $\mathcal{F}_2^{\rm last}(\vartheta)$ is obtained using

$$\mathcal{F}_2^{\rm last}(\vartheta) = \lim_{\phi\to\pi}\Re\,\widetilde{\mathcal{F}}_2^{\rm last}(\kappa = {\rm e}^{i\phi}/\vartheta)\ , \tag{21}$$

which follows from Eqs. (16) and (4) [51]. Integrals in Eq. (20) converge for $\Lambda\to\infty$ leading to the result shown in the middle of Fig. 4.

Similar calculations for the other two probabilities $P_+(\vartheta)$ and $P_{\rm max}(\vartheta)$ are more involved. For example, in $p_{\rm max}(\vartheta)$ ten diagrams contribute to the power-law $[\vartheta(1-\vartheta)]^{-H}$ in Eq. (5); in addition there are seven diagrams which contribute to $\mathcal{F}_2^{\rm max}$. All these terms need to be grouped with the appropriate repeated first-order diagrams to yield combinations which converge for $\Lambda\to\infty$. These calculations will be reported elsewhere [48].

To summarize: we calculated the probabilities (3)-(5) generalizing the three arcsine laws to fBm up to order ε^2, improved by incorporating the exact scaling results for $\vartheta\to 0$ and 1. Our numerical simulations confirm these highly non-trivial predictions accurately.

Most realizations of fBm found in practical applications fall within the range $H\simeq\frac12\pm 0.3$ where our formulas yield high-precision predictions. Our approach further offers a systematic framework to obtain other analytical results for non-Markovian processes, of which very few are available so far.

We thank J. Klamser, P. Krapivsky, S.N. Majumdar and A. Rosso for stimulating discussions, and PSL for support by grant ANR-10-IDEX-0001-02-PSL. This research was supported in part by ICTS (Code: ICTS/Prog-NESP/2015/10).

[1] P. Lévy, *Sur certains processus stochastiques homogènes*, Compositio Mathematica **7** (1940) 283–339.

[2] W. Feller, *Introduction to Probability Theory and Its Applications*, John Wiley & Sons, 1950.

[3] P. Mörters and Y. Peres, *Brownian Motion*, Cambridge University Press, 2010.

[4] Ju-Yi Yen and M. Yor, *Paul Lévy's arcsine Laws*, Springer International Publishing, Cham, 2013.

[5] S. N. Majumdar, J. Randon-Furling, M. J. Kearney and M. Yor, *On the time to reach maximum for a variety of constrained Brownian motions*, J. Phys. A **41** (2008) 365005.

[6] S. N. Majumdar and J. P. Bouchaud, *Optimal time to sell a stock in the Black-Scholes model: comment on 'Thou shalt buy and hold', by A. Shiryaev, Z. Xu and X. Y. Zhou*, Quantitative Finance **8** (2008) 753–760.

[7] J. Randon-Furling and S. N. Majumdar, *Distribution of the time at which the deviation of a Brownian motion is maximum before its first-passage time*, J. Stat. Mech. (2007) P10008.

[8] S. N. Majumdar, *Universal first-passage properties of discrete-time random walks and Lévy flights on a line: Statistics of the global maximum and records*, Physica A **389** (2010) 4299–4316.

[9] G. Schehr and P. le Doussal, *Extreme value statistics from the real space renormalization group: Brownian motion, Bessel processes and continuous time random walks*, J. Stat. Mech (2010) P01009.

[10] K. J. Hochberg and E. Orsingher, *The arcsine law and its analogs for processes governed by signed and complex measures*, Stoch. Proc. App. **52** (1994) 273–292.

[11] J. Pitman and M. Yor, *Arcsine laws and interval partitions derived from a stable subordinator*, Proc. London Math. Soc (1992) 65–326.

[12] P. Carmona, F. Petit and M. Yor, *Some extensions of the arcsine law as partial consequences of the scaling property of Brownian motion*, Prob. Theo. Rel. Fields **100** (1994) 1–29.

[13] J. Lamperti, *An occupation time theorem for a class of stochastic processes*, Trans. Am. Math. Soc. **88** (1958) 380–387.

[14] M. Barlow, J. Pitman and M. Yor, *Une extension multidimensionnelle de la loi de l'arc-sinus*, in *Siminaire de Probabilites XXIII*, pages 294–314, Springer, Berlin, 1989.

[15] N. H. Bingham and R. A. Doney, *On higher-dimensional analogues of the arcsine law*, J. App. Prob. **25** (1988) 120–131.

[16] P. A. Ernst and L. Shepp, *On occupation times of the first and third quadrants for planar Brownian motion*, J. Appl. Prob. **54** (2017) 337–342.

[17] D. Charles and W. Rosemarie, *The arcsine law and the treasury bill futures market*, Financial Analysts Journal **36** (1980) 71–74.

[18] J. Baz and G. Chacko, *Financial Derivatives: Pricing, Applications, and Mathematics*, Cambridge University Press, 2004.

[19] A. Clauset, M. Kogan and S. Redner, *Safe leads and lead changes in competitive team sports*, Phys. Rev. E **91** (2015) 062815–062826.

[20] B. B. Mandelbrot and J. W. Van Ness, *Fractional Brownian motions, fractional noises and applications*, SIAM Review **10** (1968) 422–437.

[21] G. M. Molchan, *Maximum of a fractional Brownian motion: Probabilities of small values*, Communications in Mathematical Physics **205** (1999) 97–111.

[22] J. Krug, H. Kallabis, S. N. Majumdar, S. J. Cornell, A. J. Bray and C. Sire, *Persistence exponents for fluctuating interfaces*, Phys. Rev. E **56** (1997) 2702–2712.

[23] T Guérin, N Levernier, O Bénichou and R Voituriez, *Mean first-passage times of non-Markovian random walkers in confinement*, Nature **534** (2016) 356–359.

[24] L. Decreusefond and A. S. Üstünel, *Fractional Brownian motion: Theory and applications*, in *ESAIM: PROC*, pages 75–86, 1998.

[25] P. L. Krapivsky, K. Mallick and T. Sadhu, *Dynamical properties of single-file diffusion*, J. Stat. Mech. (2015) P09007, arXiv:**1505.01287**.

[26] T. Sadhu and B. Derrida, *Large deviation function of a tracer position in single-file diffusion*, J. Stat. Mech. (2015) P09008.

[27] T. Sadhu and B. Derrida, *Correlations of the density and of the current in non-equilibrium diffusive systems*, J. Stat. Mech. (2016) 113202.

[28] A. Zoia, A. Rosso and S.N. Majumdar, *Asymptotic behavior of self-affine processes in semi-infinite domains*, Phys. Rev. Lett. **102** (2009) 120602.

[29] J. L. A. Dubbeldam, V. G. Rostiashvili, A. Milchev and T. A. Vilgis, *Fractional Brownian motion approach to polymer translocation: The governing equation of motion*, Phys. Rev. E **83** (2011) 011802.

[30] V. Palyulin, T. Ala-Nissila and R. Metzler, *Polymer translocation: The first two decades and the recent diversification*, Soft Matter **10** (2014) 9016–9037.

[31] J.-P. Bouchaud and A. Georges, *Anomalous diffusion in disordered media: Statistical mechanisms, models and physical applications*, Phys. Rep. **195** (1990) 127–293.

[32] E. E. Peters, *Chaos and order in the capital markets*, Wiley finance editions, Wiley, New York, 2 edition, 1996.

[33] N.J. Cutland, P.E. Kopp and W. Willinger, *Stock price returns and the Joseph effect: A fractional version of the Black-Scholes model*, in E. Bolthausen, M. Dozzi and F. Russo, editors, *Seminar on Stochastic Analysis, Random Fields and Applications*, Volume *36* of *Progress in Probability*, pages 327–351, Birkhäuser Basel, 1995.

[34] F. Biagini, Y Hu, B. Oksendal and T. Zhang, *Stochastic Calculus for Fractional Brownian Motion and Applications*, Springer Verlag, London, 2008.

[35] T. Sottinen, *Fractional Brownian motion, random walks and binary market models*, Finance and Stochastics **5** (2001) 343–355.

[36] B.B. Mandelbrot and J.R. Wallis, *Noah, Joseph, and operational hydrology*, Water Resources Research **4** (1968) 909–918.

[37] S. Gupta, A. Rosso and C. Texier, *Dynamics of a tagged monomer: Effects of elastic pinning and harmonic absorption*, Phys. Rev. Lett. **111** (2013) 210601.

[38] E. Monte-Moreno and M. Hernández-Pajares, *Occurrence of solar flares viewed with GPS: Statistics and fractal nature*, J. Geophys. Res. **119** (2014) 9216–9227.

[39] I. Simonsen, *Measuring anti-correlations in the nordic electricity spot market by wavelets*, Physica A **322** (2003) 597–606.

[40] I. Norros, *On the use of fractional Brownian motion in*

the theory of connectionless networks, IEEE J. Sel. A. Commun. **13** (2006) 953–962.

[41] K. Burnecki, E. Kepten, J. Janczura, I. Bronshtein, Y. Garini and A. Weron, *Universal algorithm for identification of fractional Brownian motion. A case of telomere subdiffusion*, Biophysical Journal **103** (2012) 1839–1847.

[42] D. Ernst, M. Hellmann, K. Jürgen and M. Weiss, *Fractional Brownian motion in crowded fluids*, Soft Matter **8** (2012) 4886–4889.

[43] M. Delorme and K.J. Wiese, *The maximum of a fractional Brownian motion: Analytic results from perturbation theory*, Phys. Rev. Lett. **115** (2015) 210601, arXiv:**1507.06238**.

[44] M. Delorme and K.J. Wiese, *Perturbative expansion for the maximum of fractional Brownian motion*, Phys. Rev. E **94** (2016) 012134, arXiv:**1603.00651**.

[45] M. Delorme and K.J. Wiese, *Extreme-value statistics of fractional Brownian motion bridges*, Phys. Rev. E **94** (2016) 052105, arXiv:**1605.04132**.

[46] M. Delorme, *Stochastic processes and disordered systems, around Brownian motion*, PhD thesis, PSL Research University, 2016.

[47] A. B. Dieker, *Simulation of fractional Brownian motion*, PhD thesis, University of Twente, 2004.

[48] T. Sadhu and K.J. Wiese, to be published.

[49] K.J. Wiese, S.N. Majumdar and A. Rosso, *Perturbation theory for fractional Brownian motion in presence of absorbing boundaries*, Phys. Rev. E **83** (2011) 061141, arXiv:**1011.4807**.

[50] The action is written in a form that when evaluating it in perturbation theory, so-called "contact-terms" proportional to δ functions in time from the contraction of two $\dot{X}$ have to be discarded.

[51] It contains the real part $\Re$, as it is divided by the order-0 result (18).

Supplementary Material: Result for $\mathcal{F}_2$

The analytical expressions for $\mathcal{F}_2$ are quite complicated, and contain as Eq. (20) numerical integrals to be performed. In order that the reader can use our results, we give simple approximations to the results obtained after numerical integration of these integrals, which fit the analytical formulas to a good extent.

$$\mathcal{F}_2^{+}(\vartheta) \simeq -0.842235 + 1.76479\,[\vartheta(1-\vartheta)]^{\frac{1}{2}} + 3.70810\,[\vartheta(1-\vartheta)] - 9.71973\,[\vartheta(1-\vartheta)]^{\frac{3}{2}} + 7.40511\,[\vartheta(1-\vartheta)]^{2} \quad \text{(S1)}$$

$$\mathcal{F}_2^{\text{last}}(\vartheta) \simeq -17.92401 + 13.30207\sqrt{\vartheta} - 2.16604\sqrt{1-\vartheta} + 8.30059\vartheta + 11.59529\vartheta^{\frac{3}{2}} + 13.23121(1-\vartheta)^{\frac{3}{2}} - 10.74274\vartheta^{2} \quad \text{(S2)}$$

$$\mathcal{F}_2^{\max}(\vartheta) \simeq -0.431001 + 1.69259\,[\vartheta(1-\vartheta)]^{\frac{1}{2}} - 1.93367\,[\vartheta(1-\vartheta)] + 1.3572\,[\vartheta(1-\vartheta)]^{\frac{3}{2}} - 0.33995\,[\vartheta(1-\vartheta)]^{2} \quad \text{(S3)}$$

Note that $\mathcal{F}_2^{+}(\vartheta)$ and $\mathcal{F}_2^{\max}(\vartheta)$ are symmetric under the exchange of $\vartheta \to 1-\vartheta$ while $\mathcal{F}_2^{\text{last}}(\vartheta)$ is not.